Supplementary Information

Precursor-Engineered Prelithiation Strategy $CaMoO_4$ enhancing ion transport in Composite Solid Electrolytes for Flexible Interdigitated Micro-Supercapacitors

Haoyu Wu, [a] N. Fairuz Zaini Ambia,[b] Nurdiana Nordin *[b] and S.R. Majid *[a]

a.Department of Physics, Faculty of Science, Universiti Malaya, 50603, Kuala Lumpur, Malaysia

b.Department of Chemistry, Faculty of Science, Universiti Malaya, 50603, Kuala Lumpur, Malaysia.

List of supplementary information

1. Supplementary table: TableS1-TableS5
2. Supplementary figure: Figure S1-Figure S6
3. Supplementary Note: Note1-Note2

Table S1 Compositions of PVDF-HFP/$LiCF_3SO_3$/Li–$CaMoO_4$ composite polymer electrolytes

Sample	A-Li-$CaMoO_4$ (wt.%)	B-Li-$CaMoO_4$ (wt.%)	PVDF-HFP (g)	$LiCF_3SO_3$ (g)
S1	0	0	0.3	0.2
A-S2	10	0	0.3	0.2
A-S3	20	0	0.3	0.2
A-S4	30	0	0.3	0.2
B-S2	0	10	0.3	0.2
B-S3	0	20	0.3	0.2
B-S4	0	30	0.3	0.2
B-S5	0	40	0.3	0.2
B-S6	0	50	0.3	0.2

Table S2 specific capacitance of supercapacitor with A-S2 at different condition

A-S2		
Voltage range (V)	Scan rate (mV/S)	Capacitance (F/g)
0-0.6	10	10.5
0-1.0	10	18.0
0-1.4	10	20.7
0-1.8	10	25.0
0-2.2	10	30.3
0-1.0	5	51.2
0-1.0	20	31.3
0-1.0	50	20.0
0-1.0	100	14.7

Table S3 specific capacitance of supercapacitor with S1 at different condition

S1		
Voltage range (V)	Scan rate (mV/S)	Capacitance (F/g)
0-0.6	10	7.3
0-1.0	10	11.6
0-1.4	10	17.4
0-1.8	10	24.4
0-2.2	10	23.2
0-1.0	5	41.2
0-1.0	20	25.4
0-1.0	50	17.8
0-1.0	100	12.9

Table S4 Comparison our PVDF-HFP/ Li-CaMoO4 micro-capacitor with other reported micro-capacitors

Reference	Activated material	Electrolyte	Impedance (Ω)	Cycling retention (%)	Capacitance (mF cm^{-2})	Capacitance Retention (Bent/Flat)	Energy Density (μWh cm^{-2})	Power Density (μW cm^{-2})
Our work	Activated carbon	PVDF-HFP/ Li-$CaMoO_4$	26 Ω	91 after 10,000 cycle	36.9	98.6	3.28	196.8
S1	Activated carbon	LiTFS–LiSMC	500 Ω	96 after 20,000 cycle	0.41	75.9	0.036	2.60
S2	PPD grafted rGO electrode	H_2SO_4 /PVA	2.1 Ω	64 after 10,000 cycle	38.4	N/A	4.4	44.6
S3	Microporous graphene	H_2SO_4	205 Ω	84 after 5000 cycle	16	97	5.8	1
S4	CNT/PANI	PVA/H_3PO_4	45.5 Ω	80 after 5000 cycle	19.74	99	17.8	63
S5	graphene	PVA/KOH	1.18 Ω	98.1 after 5000 cycle	50.9	94.2	2.2	5

Table S5 ICP-OES results of A-Li-$CaMoO_4$ and B-Li-$CaMoO_4$

Sample	Element	Dilution Factor	C_0 (mg/L)	Content
A-Li-$CaMoO_4$	Li	100	3.0461	5.4885%
A-Li-$CaMoO_4$	Mo	100	17.6115	31.7325%
B-Li-$CaMoO_4$	Li	100	0.6428	1.0556%
B-Li-$CaMoO_4$	Mo	100	25.1230	40.8649%

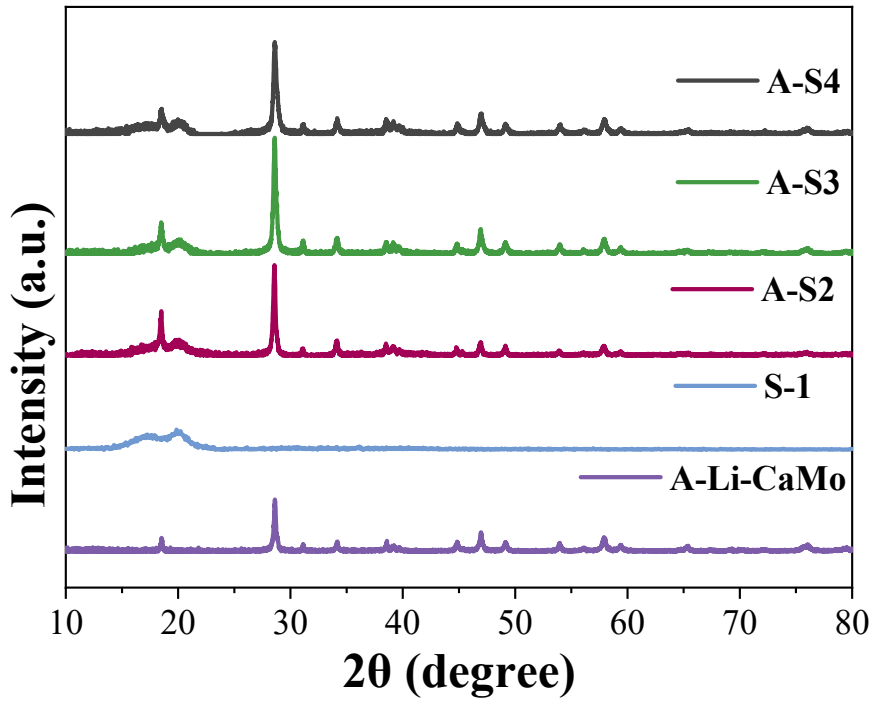

Figure S1 The XRD patterns of S1, A-S2, A-S3, A-S4 and A-Li-CaMo

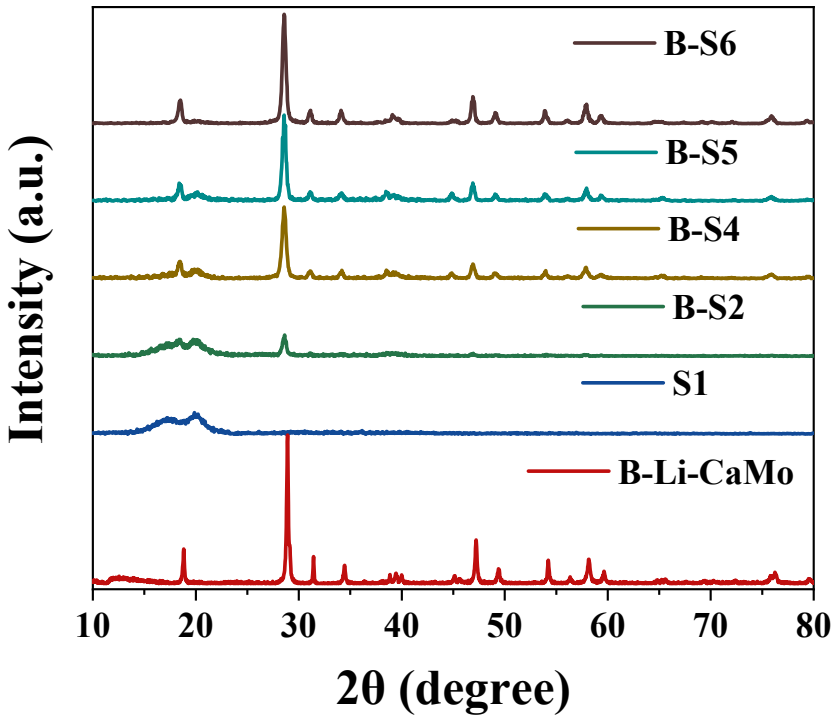

Figure S2 The XRD patterns of S1, B-S2, B-S3, B-S4, B-S5, B-S6 and B-Li-CaMo

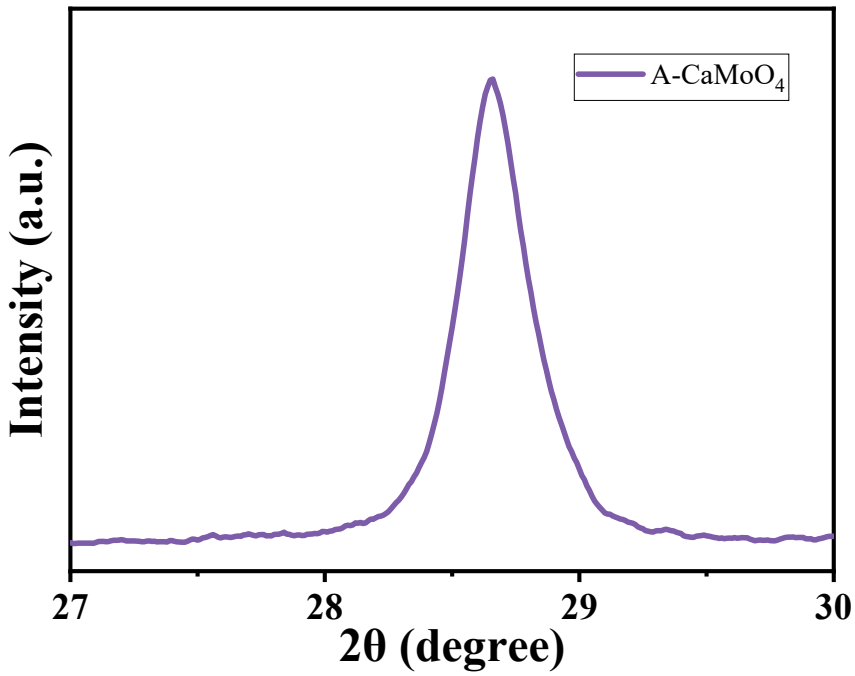

Figure S3 The enlarged XRD pattern of A-CaMoO4's (112) peak(~28°)

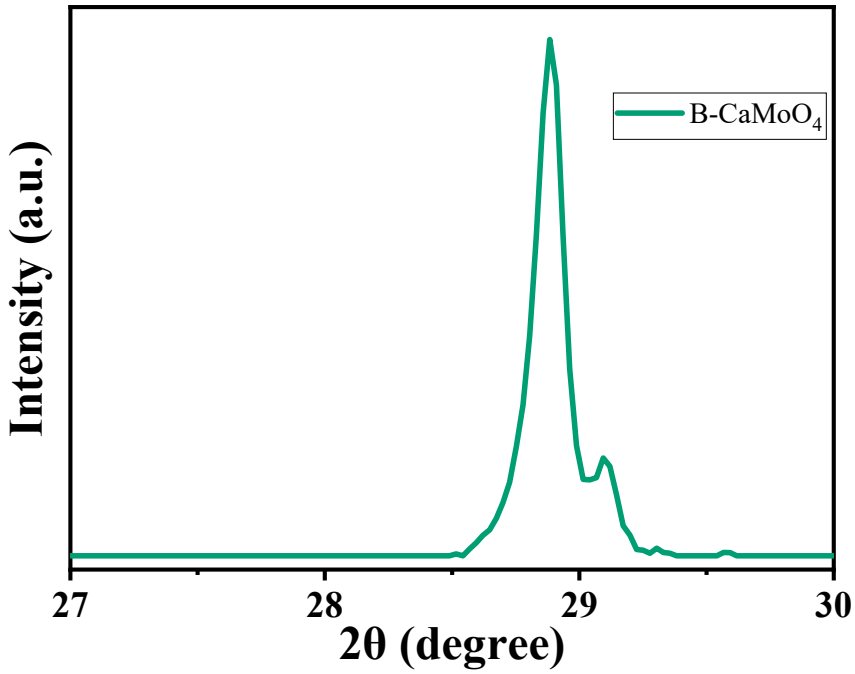

Figure S4 The enlarged XRD pattern of A-CaMoO4's (112) peak(~28°)

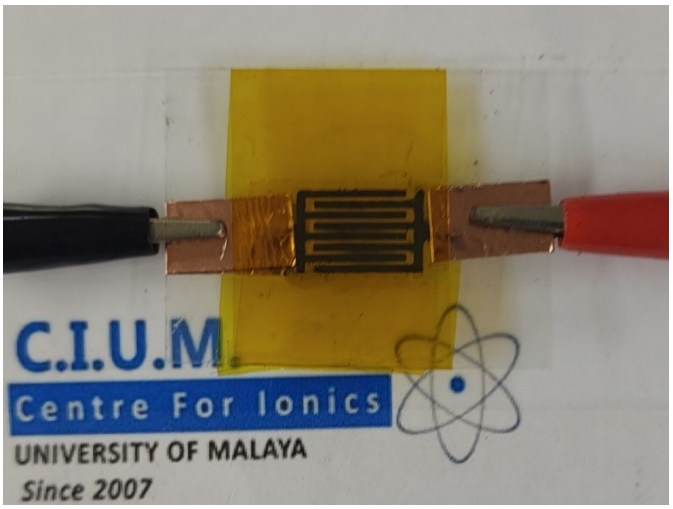

Figure S5 the digital image of micro-supercapacitor in flat condition

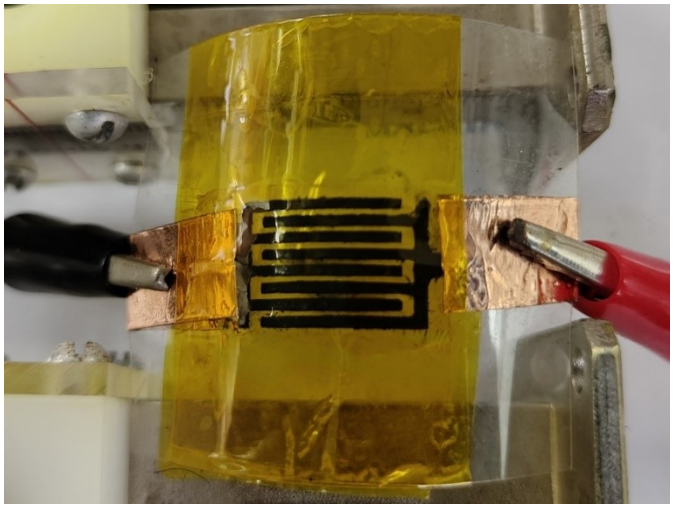

Figure S6 the digital image of micro-supercapacitor in bent condition

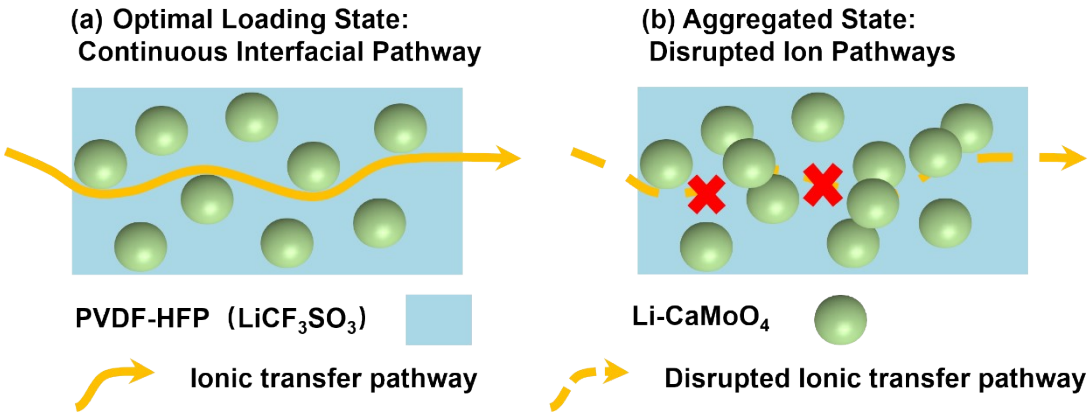

Figure S7 Schematic illustration of Li^+ transport pathways. (a) Uniform filler dispersion at optimal loading forms a continuous conducting network. (b) Excessive filler aggregation disrupts the network and impedes ion transport.

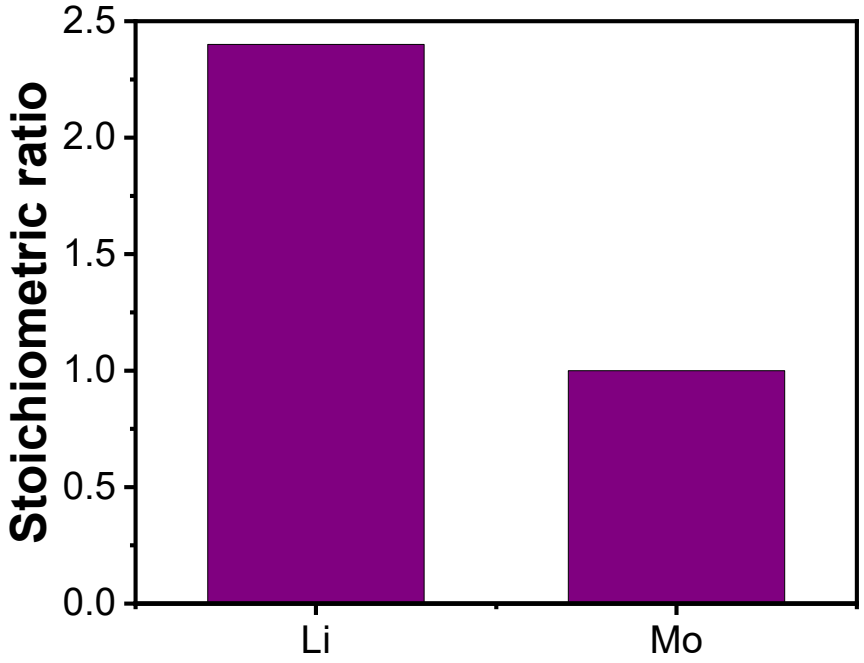

Figure S8 ICP-OES of A-Li-$CaMoO_4$

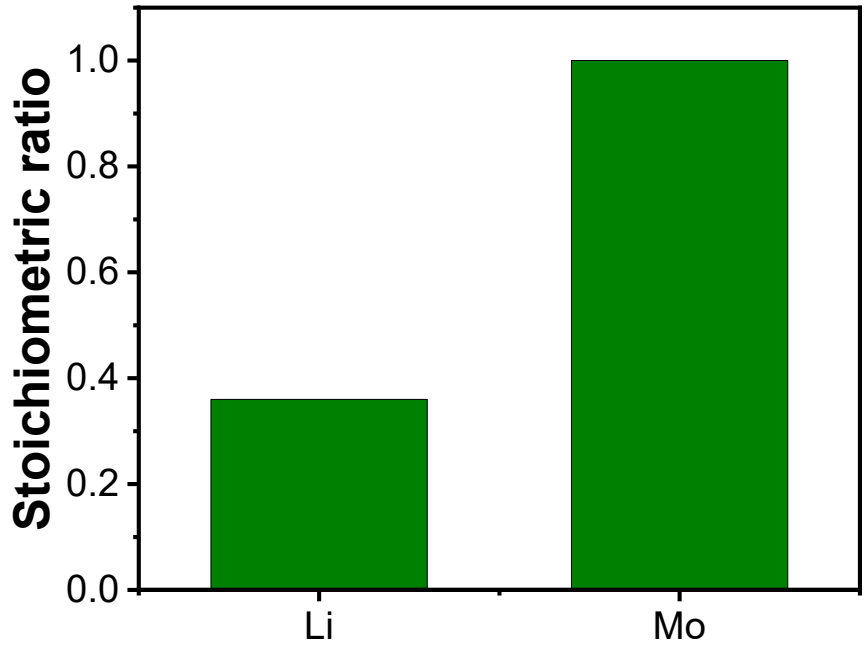

Figure S9 ICP-OES of B-Li-$CaMoO_4$

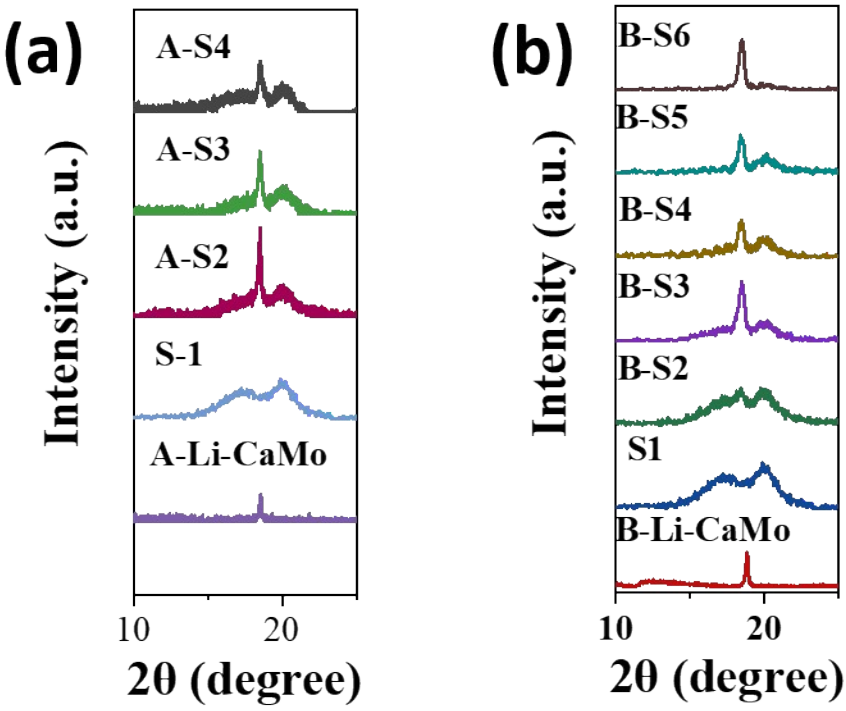

Figure S10 Zoomed in A system and B system's XRD patterns in the range between 10°and 25°

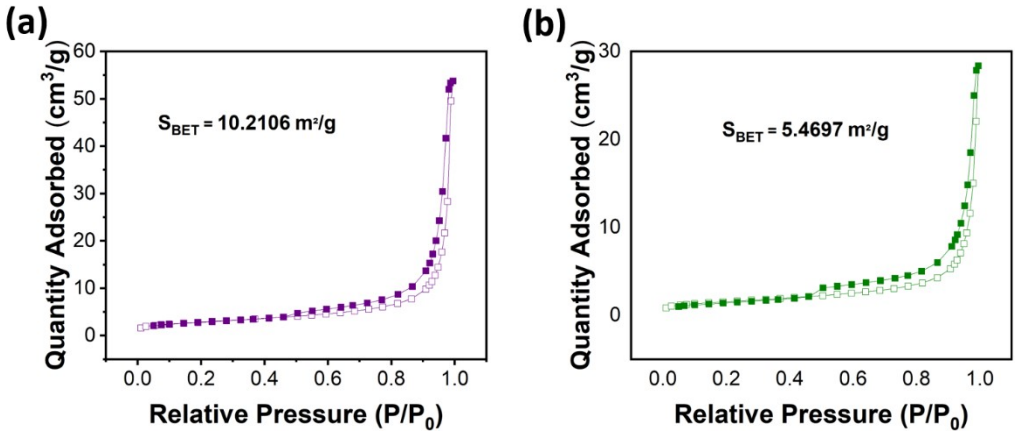

Figure S11 N_2 adsorption–desorption isotherms taken on (a) A-$CaMoO_4$ and (b) B-$CaMoO_4$

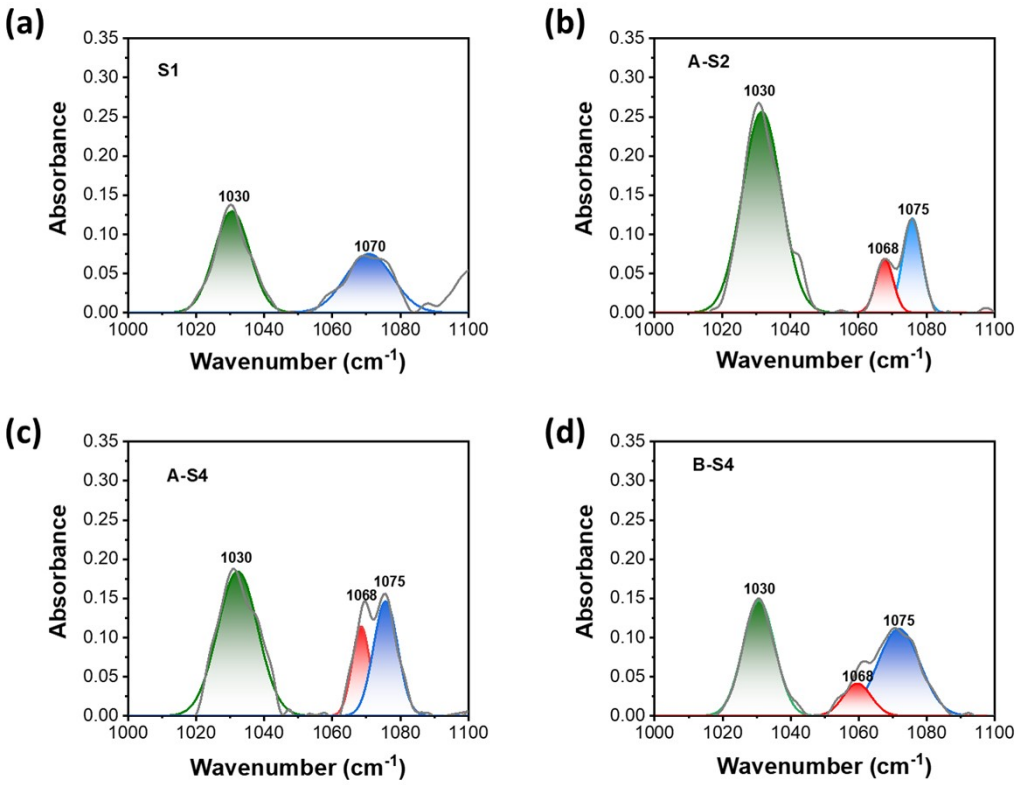

Figure S12 Enlarged FTIR spectra (1000–1100 cm^{-1}) and corresponding peak deconvolution results for S1, A-S2, A-S4, and B-S4.

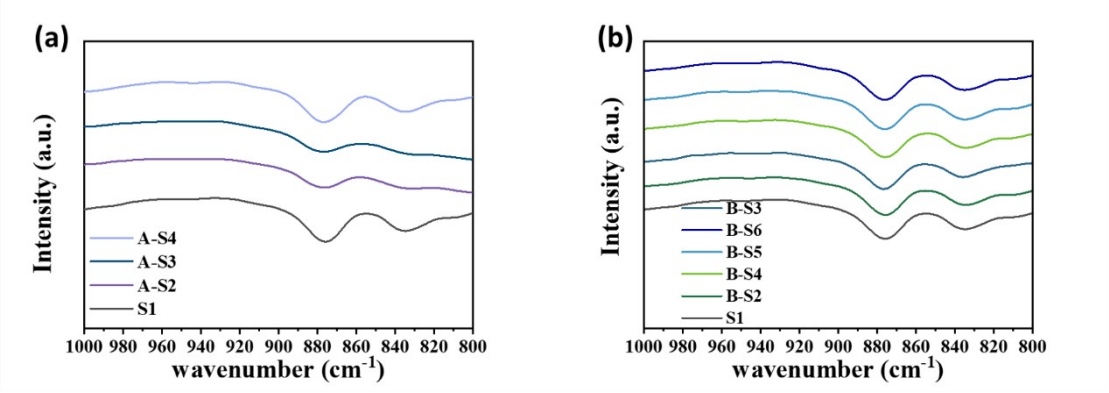

Figure S13 Enlarged FTIR spectra (1000–800 cm^{-1})

Note 1： Mechanistic Insight into Li^+ Accommodation and Space-Charge Mitigation

The interface between the organic polymer matrix and inorganic fillers is typically the site of a significant electrochemical potential mismatch. This thermodynamic disparity drives the redistribution of charge carriers, creating a space-charge layer characterized by a localized depletion of charge carriers, which acts as a high-resistance barrier to ion transport.

To overcome this barrier, prelithiation is employed as a critical interfacial engineering strategy. By chemically accommodating mobile lithium ions within the $CaMoO_4$ host structure, this process achieves two synergistic effects[S7]:

1. Potential Equalization: The presence of pre-intercalated lithium modifies the Fermi level of the filler, reducing the potential gradient across the polymer-filler interface and suppressing the formation of the depletion zone.
2. Reservoir Effect: The lithiated host structure functions as a dynamic lithium ion reservoir. This ensures a continuous supply of mobile ions directly at the interface, effectively bridging the transport pathway between the ceramic and polymer phases.

Note 2: Mechanism of Filler Aggregation and Ion Transport

To further elucidate the impedance trends observed in Figure 2, we provide a schematic illustration of the ion transport mechanism relative to filler dispersion (Figure S7).

According to the percolation theory, the ionic conductivity in composite polymer electrolytes is heavily dependent on the connectivity of the highly conductive interphase regions formed between the polymer matrix and the inorganic fillers[S8]. As illustrated in Figure S7a, at the optimal loading fillers create a continuous and providing low-resistance pathways for fast Lithium ion migration.

However, as shown in Figure S7b, when the filler content exceeds the percolation threshold, excessive aggregation occurs. This aggregation has two detrimental effects:

1. Loss of Active Interface: The formation of large clusters reduces the effective specific surface area of the fillers, diminishing the volume of the conductive interfacial layer.
2. Pathway Tortuosity: The agglomerates act as insulating blocks that disrupt the continuous transport network, forcing Lithium ions to take more tortuous paths through the highly resistive bulk polymer regions, thereby increasing the overall impedance.

Supplementary References:

S1. Kim, S. K., Yoon, Y., Ryu, J. H., Kim, J. H., Ji, S., Song, W., ... & An, K. S. (2020). Recyclable High-Performance Polymer Electrolyte Based on a Modified Methyl Cellulose–Lithium Trifluoromethanesulfonate Salt Composite for Sustainable Energy Systems. *ChemSusChem*, *13*(2), 376-384.

S2. Ravichandran, V., Nardekar, S. S., Kesavan, D., Das, J. P., Elumalai, V., & Kim, S. J. (2024). High-performance redox-active organic molecule grafted graphene based on-chip micro-supercapacitor towards self-powered environmental monitoring station. *Chemical Engineering Journal*, *482*, 148822.

S3. Kim, M., Gu, M. G., Jeong, H., Song, E., Jeon, J. W., Huh, K. M., ... & Kim, B. G. (2020). Laser scribing of fluorinated polyimide films to generate microporous structures for high-performance micro-supercapacitor electrodes. *ACS Applied energy materials*, *4*(1), 208-214.

S4. Wang, X., Liu, Y., Li, H., Lv, T., Wan, J., Dong, K., ... & Chen, T. (2021). Regulating the self-discharge of flexible all-solid-state supercapacitors by a heterogeneous polymer electrolyte. *Small*, *17*(31), 2102054.

S5. Chen, S., Sun, H., Chen, Y., Fang, Q., Huang, Z., Liu, Y., ... & Cao, D. (2024). Facile Preparation of High-Performance Free-Standing Micro-Supercapacitors by Optimizing Oxygen Groups on Graphene. *Small*, *20*(49), 2404307.

S6. Architha, M., Neena, P. K., Punnakkal, N., Babu, T. S., & Suneesh, P. V. (2025). Fabrication of high cycling stability flexible micro-supercapacitor using electrodeposited polyaniline-nitrogen sulphur doped carbon dot binary nanocomposites. *Electrochimica Acta*, 146518.

S7. Shi, P., Ma, J., Liu, M., Guo, S., Huang, Y., Wang, S., ... & Kang, F. (2023). A dielectric electrolyte composite with high lithium-ion conductivity for high-voltage solid-state lithium metal batteries. Nature Nanotechnology, 18(6), 602-610.

S8. Li, Z., Huang, H. M., Zhu, J. K., Wu, J. F., Yang, H., Wei, L., & Guo, X. (2018). Ionic conduction in composite polymer electrolytes: case of PEO: Ga-LLZO composites. *ACS applied materials & interfaces*, *11*(1), 784-791.